Entropy Generation and Dual Solutions in Mixed Convection Stagnation Point Flow of Micropolar Ti6Al4V Nanoparticle along a Riga Surface

Authors:

A. Zaib, Umair Khan, Ilyas Khan, Asiful H. Seikh, El-Sayed M. Sherif

Date Submitted: 2020-02-03

Keywords: thermal radiation, titanium alloy nanomaterial, Riga plate, micropolar fluid, dual solution, entropy generation

Abstract:

Entropy generation and dual solutions are rarely studied in the literature. An analysis is attempted here. More exactly, the present paper looks at the impact of radiation of a micropolar fluid on mixed convective flow containing the titanium alloy Ti6Al4V nanoparticle along with a Riga plate. The study of dual-nature solution for the entropy generation along a Riga surface was not being explored in the literature; therefore, the current model focuses on the dual solutions of this complex nature model. Riga surface is identified as an actuator of electromagnetic in which electrodes are accumulated alternatively. This array produces the behavior of electromagnetic hydrodynamic in the flow field. The transmuted leading equations were worked out through the formula of 3-stage Lobatto IIIA. Influences of exercising enormous parameters on temperature distribution, velocity, and micro rotation fields are portrayed and argued. More than one solution is achieved in opposing flow, while in the phenomenon of assisting flow result is unique. Moreover, due to the micropolar parameter, the separation of the boundary layer is decelerating. It is determined that the entire structure produces the dual-nature solution of the phenomenon of stagnation point flow, and the temperature profile behavior shows the significant enhancement in the thermal conductivity due to the addition of the nanoparticle. The results exposed that liquid velocity is enhanced, and micro rotation is decelerated, by improving the values of Hartmann numbers in both solutions, whereas the temperature field is decelerated in the first solution and accelerated in the second solution.

Record Type: Published Article

Submitted To: LAPSE (Living Archive for Process Systems Engineering)

Citation (overall record, always the latest version):	LAPSE:2020.0170
Citation (this specific file, latest version):	LAPSE:2020.0170-1
Citation (this specific file, this version):	LAPSE:2020.0170-1v1

DOI of Published Version: https://doi.org/10.3390/pr8010014

processes

MDPI

Article

Entropy Generation and Dual Solutions in Mixed Convection Stagnation Point Flow of Micropolar Ti_6Al_4V Nanoparticle along a Riga Surface

A. Zaib [1], Umair Khan [2], Ilyas Khan [3,*], Asiful H. Seikh [4] and El-Sayed M. Sherif [4,5]

1 Department of Mathematical Sciences, Federal Urdu University of Arts, Science & Technology, Gulshan-e-Iqbal Karachi 75300, Pakistan; aurangzaib@fuuast.edu.pk
2 Department of Mathematics and Social Sciences, Sukkur IBA University, Sukkur 65200, Sindh, Pakistan; umairkhan@iba-suk.edu.pk
3 Faculty of Mathematics and Statistics, Ton Duc Thang University, Ho Chi Minh City 72915, Vietnam
4 Center of Excellence for Research in Engineering Materials (CEREM), King Saud University, P.O. Box 800, Al-Riyadh 11421, Saudi Arabia; aseikh@ksu.edu.sa (A.H.S.); esherif@ksu.edu.sa (E.-S.M.S.)
5 Electrochemistry and Corrosion Laboratory, Department of Physical Chemistry, National Research Centre, El-Behoth St. 33, Dokki, Cairo 12622, Egypt
* Correspondence: ilyaskhan@tdtu.edu.vn

Received: 11 November 2019; Accepted: 15 December 2019; Published: 20 December 2019

Abstract: Entropy generation and dual solutions are rarely studied in the literature. An analysis is attempted here. More exactly, the present paper looks at the impact of radiation of a micropolar fluid on mixed convective flow containing the titanium alloy Ti_6Al_4V nanoparticle along with a Riga plate. The study of dual-nature solution for the entropy generation along a Riga surface was not being explored in the literature; therefore, the current model focuses on the dual solutions of this complex nature model. Riga surface is identified as an actuator of electromagnetic in which electrodes are accumulated alternatively. This array produces the behavior of electromagnetic hydrodynamic in the flow field. The transmuted leading equations were worked out through the formula of 3-stage Lobatto IIIA. Influences of exercising enormous parameters on temperature distribution, velocity, and micro rotation fields are portrayed and argued. More than one solution is achieved in opposing flow, while in the phenomenon of assisting flow result is unique. Moreover, due to the micropolar parameter, the separation of the boundary layer is decelerating. It is determined that the entire structure produces the dual-nature solution of the phenomenon of stagnation point flow, and the temperature profile behavior shows the significant enhancement in the thermal conductivity due to the addition of the nanoparticle. The results exposed that liquid velocity is enhanced, and micro rotation is decelerated, by improving the values of Hartmann numbers in both solutions, whereas the temperature field is decelerated in the first solution and accelerated in the second solution.

Keywords: entropy generation; dual solution; micropolar fluid; Riga plate; titanium alloy nanomaterial; thermal radiation

1. Introduction

The topic of non-Newtonian liquid is a defying and inspiring area, as it encloses plenty of imperative problems from the processing of biomedical food, petroleum, polymer, and chemical industries. Models of non-Newtonian liquids are relatively valuable to exemplify the flow of commonly used liquids, existing naturally or processed, like slurries, motor oils, volcano lava, biological liquids, paste, and polymer liquids. The dilute suspensions macro-molecules rigid through motion were grasped by micropolar fluid and their individual body moment and stress which are related to spin

inertia. The theory of micropolar fluid was introduced by Eringen [1]; it describes a group of fluids that demonstrated certain characters of microscopic occurring from micro-rotation and the local formation of the liquid components. These liquids include dilute suspensions of rigid macro-molecules through motions of individuals that carry the stress and moment of the body which are affecting through spin inertia. Mohammadein and Gorla [2] investigated the impact of viscous dissipation on liquid motion of micropolar liquid from an expanded sheet with heat generation. The time-dependent mixed convective flow near a stagnation-point involving non-Newtonian micropolar liquid through a vertical surface was examined by Lok et al. [3]. They discussed the assisting flow, as well as opposing flow, of the cases of small-time and large-time solutions. Aman et al. [4] scrutinized the impacts of slips on mixed convective flow toward a stagnation point through a vertical sheet. They observed that the multiple solutions are attained for a certain amount of buoyancy constraint for opposing flow only, while the solution is unique in the case of assisting flow. Turkyilmazoglu [5] discussed the characteristic of heat transfer involving micropolar fluid from a permeable stretching sheet. Analytic solution of unsteady flow of micropolar liquid by Newtonian heating was found by Hussanan et al. [6]. Waqas et al. [7] explored the influence of magnetohydrodynamics (MHD) flow of micropolar liquid through moving sheet along forced convection, thermal radiation, and heat flux. Das and Duari [8] inspected the influence of chemical reaction on the liquid movement of micropolar liquid containing nanomaterial from an overextended sheet. Combined possessions of MHD and viscous dissipation on liquid flow of micropolar liquid containing nanofluid to a stretched surface were scrutinized by Hsiao [9]. Recently, the analytical solution of micropolar liquid through mass and heat transfer by Newtonian heating was explored by Hussanan et al. [10].

A metallic liquid or solid that may be compiled from a combination of homogenous/non-homogenous of two or more metalloid either nonmetals or metal nanometer size elements are known as a mixture. In modern times, they can be utilized in order to convey the definite physical character of mixtures. The examples of alloys are gold, steel brass, solder, and phosphor bronze. Alloys have been used in a variety of applications, e.g., technologies in aerospace science and advanced powder, processes of a hip-joint substitute, implantation through surgery, and many biological treatments. In addition, alloys are employed in the handling of fabrication systems, production of hot and cold rolled sheets, and many more. These alloys also maintain the savings weight in model of smaller strengthen the place of aerospace type steel and aluminum. More about alloys and their applications can be seen in [11–13]. Afterward, many researchers [14–18] showed the theoretical, as well as experimental, explorations with different effects and geometries on flow of titanium alloys. In addition, in the equipment of heat transfer, liquids are frequently used as heat transporters [19,20].

In equipment of heat transfer, liquids are frequently used as heat transporters. For example, heat transfer liquid shows a vital responsibility in numerous manufacturing applications in engineering, such as polymer, microelectronic, and automotive industries. In the heat-transfer process, thermal conductivity of liquids is significant in the equipment of the transfer rate of heat at the surface [21,22]. However, the regular heat transported of solutions, such as oil, toluene, and water, is generally insufficient for the rate of transferring heat. The thermal conductivity of a metallic solid like gold is greater compared to regular liquid, like oil. Thus, metallic fluids have extra thermal conductivity associated with nonmetallic fluids. As a result, several researchers endeavored to dispense metallic solid/liquid particles in regular liquids, to improve the heat-transfer rate and thermal conductivity. Maxwell [23] showed that the thermal conductivity of nanoparticles improved due to solid particles of volume fraction, taking into account the spherical particles in the analysis of flow. However, when micro and mini-sized particles merge with the regular fluids, the liquid flows can have blockage problems. Consequently, extremely small amount of particles is required to dispense in the solutions, to make them free of blockage troubles. Choi [24] was the first one who utilized the concept of nanofluid that submits to the liquid in which extremely small-sized (<50 nm) particles dispersed into regular liquids. However, the present technology is adequate to assemble nanoparticles of 10nm. Afterward, Pop and Khan [25] discussed the boundary layer flow containing nanoliquid from stretched

surface. Mabood et al. [26] found that water-based Al_2O_3 nanoparticles give a wider velocity boundary layer compared to water base copper nanoparticles. Nonlinear radiative heat transfer containing water-based copper and silver nanoparticles on mixed convective flow was investigated by Hayat et al. [27]. Du and Tang [28] scrutinized the properties of plasmonic optical nanoliquids involving gold nanoparticles, taking into account of different sizes and shapes. Recently, Zaib et al. [29] argued the effects of binary chemical reaction and activation energy on flow of Williamson nanoliquid through a plate with energy condition.

Flow of electrically conducting liquid, for example electrolytes, fluid rails and plasma, etc. can be managed through pertaining MHD. These flows have remarkable applications in geophysics, sensors and engineering etc. Magnetic and electric fields are required to direct and control the liquid flow. These kinds of flow are described as EMHD flow. Riga plate is one of the devices is utilized in this regard. The influence of EMHD (Electro–magneto–hydrodynamic) has an important character in act of momentum and the consequence detected in micro-coolers, thermal reactor, chromatography of liquid and controlling the flow in network of fluids. In 1861, Gallites and Lilausis [30] considered Riga surface to produce and pertained electric and magnetic fields in order to manage fluid flow which accordingly creates Lorentz force equivalent to the wall. Magyari and Pantokratoras [31] examined the flow from a Riga plate enclosing low electrical conductivity. From a Riga plate, the entropy analysis was scrutinized by Abbas et al. [32], in the presence of nanomaterials' fluid flow. The impact of chemical reaction on squeezing flow from a convectively heated Riga surface was examined by Hayat et al. [33]. Recently, Iqbal et al. [34] utilized Keller box procedure to obtain the numerical solution of melting heat-transfer flow comprising nanomaterial through the Riga surface with irregular thickness.

The idea of entropy generation is incredibly imperative to examine the problems of heat transfer. Minimization of entropy cohort has been widely wrapped by Bejan [35] particularly, in the fields of freezing, heat transfer, conversion of thermal solar power, and storage. The minimization technique of entropy generation is utilized to improve the devices of thermal manufacturing for efficiency of higher energy. Aiboud and Sauoli [36] discussed the influence of entropy generation in viscoelastic electrically conducting flow from a wide elastic sheet. The effect of velocity slip on flow toward a convectively heated vertical surface was presented by Butt et al. [37]. Noghrehabadiet al. [38] investigated the heat generation/absorption effects on fluid flow comprising nanofluid through a stretched sheet with entropy generation. Abolbashari et al. [39] scrutinized the entropy generation on the slip flow of Casson nanofluid induced by convectively heated stretched sheet. Entropy generation involving non-Newtonian Jeffrey liquid in the presence of nanomaterials induced by stretched sheet with zero flux was surveyed by Rehman et al. [40]. Recently, Azhar et al. [41] discussed the entropy generation through an unsteady MHD fractional flow of Couette liquid in a rotating frame with exponentially heating walls.

The configuration of micropolar liquid with titanium alloy nanomaterial composes the more complex mixture compared to regular nanoliquids. Therefore, we planned to explore the mixed convective flow containing micropolar titanium alloy nanomaterial from a vertical Riga plate through an entropy generation with thermal radiation. Exercising via the formula of three-stage Lobatto IIIA computationally on the established similarity equations, to find more than one result (dual solutions). The influences of the significant parameters have argued in detail through the help of the tables and the graphs.

2. Construction of Problem

The contemplate of a steady mixed convective flow near a stagnation-point involving micropolar liquid comprising water-based titanium alloy nanomaterial from a Riga plate with thermal radiation and entropy generation is scrutinized. We have considered the Cartesian coordinates x-y system, where x is taken along the Riga surface and y is normal to it. We deem that the ambient velocity and temperature are taken to be linearly $(\breve{u}_\infty(\breve{x}) = c\breve{x})$ and $\left(\breve{T}_w(\breve{x}) = \breve{T}_\infty + b\breve{x}\right)$ with $\breve{T}_w(\breve{x}) > \breve{T}_\infty$, respectively, where $\breve{T}_\infty$, c, and b correspondingly stand for the ambient temperature and positive

constants. Additionally, an irregular array of electrodes gathered with the permanent magnets on the surface of the plate presented in (Figure 1), using Riga plate. These arrays generate a resistive-type force known as the Lorentz force. This force is parallel to the plate's surface and declines exponentially in the horizontal way to the surface, after exercising via the Boussinesq approximation, along with a boundary layer approximation. The condition in the model was used to create the following leading system of equations (Equations (1) to (4)) [42,43].

$$\frac{\partial \check{v}}{\partial \check{y}} + \frac{\partial \check{u}}{\partial \check{x}} = 0 \tag{1}$$

$$\begin{gathered}\check{u}\frac{\partial \check{u}}{\partial \check{x}} - \frac{\check{\kappa}}{\check{\rho}_{nf}}\frac{\partial \check{N}}{\partial \check{y}} + \check{v}\frac{\partial \check{u}}{\partial \check{y}} - \check{u}_{\infty}\frac{d\check{u}_{\infty}}{d\check{x}} = \frac{\left(\check{\mu}_{nf}+\check{\kappa}\right)}{\check{\rho}_{nf}}\frac{\partial^2 \check{u}}{\partial \check{y}^2} + \frac{\check{\pi}\check{J}_0\check{M}_0}{8\check{\rho}_{nf}}e^{-\frac{\check{\pi}}{\check{d}}\check{y}} \\ -\frac{g\left(\check{\rho}\check{\beta}\right)_{nf}}{\check{\rho}_{nf}}\left(\check{T}_{\infty}-\check{T}\right)\end{gathered} \tag{2}$$

$$\check{u}\frac{\partial \check{N}}{\partial \check{x}} + \frac{\check{\kappa}}{\check{\rho}_{nf}\check{j}}\left(2\check{N} + \frac{\partial \check{u}}{\partial \check{y}}\right) + \check{v}\frac{\partial \check{N}}{\partial \check{y}} = \frac{\check{\gamma}_{nf}}{\check{\rho}_{nf}\check{j}}\frac{\partial^2 \check{N}}{\partial \check{y}^2} \tag{3}$$

$$\check{u}\frac{\partial \check{T}}{\partial \check{x}} + \frac{1}{\left(\check{\rho}c_p\right)_{nf}}\frac{\partial \check{q}_r}{\partial \check{y}} + \check{v}\frac{\partial \check{T}}{\partial \check{y}} = \check{\alpha}_{nf}\frac{\partial^2 \check{T}}{\partial \check{y}^2} \tag{4}$$

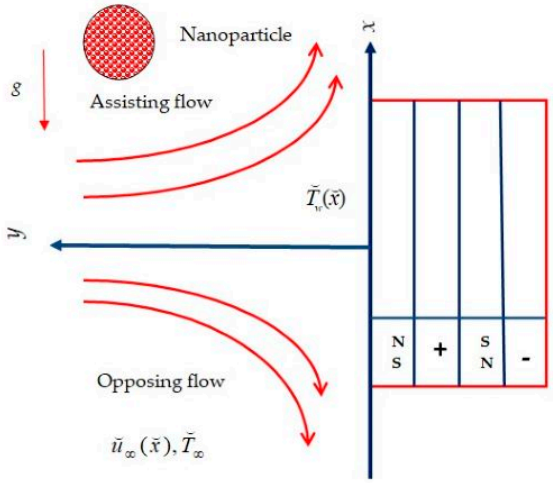

Figure 1. Physical diagram of the problem.

The physical conditions of the boundary are as follows:

$$\begin{gathered}\check{u} = 0,\ \check{T} = \check{T}_w(\check{x}),\ \check{v} = 0, \check{N} = -\check{n}\frac{\partial \check{u}}{\partial \check{y}} \text{ at } \check{y} = 0, \\ \check{u} \to \check{u}_{\infty}(\check{x}),\ \check{N} \to 0, \check{T} \to \check{T}_{\infty} \text{ as } \check{y} \to \infty.\end{gathered} \tag{5}$$

In the aforementioned equations, $\check{y}-$ and $\check{x}-$ are axes direction, and the velocity component is represented by $\check{v}$ and $\check{u}$, respectively. β_{nf}, g, J_0, d, $\check{M}_0$, $\check{\kappa}$, $\check{\rho}_{nf}$, and $\check{\mu}_{nf}$, are the nanofluid thermal expansion, acceleration caused by gravity, the applied current density in the electrodes, electrodes and magnets width, magnetization of the permanents magnets, vortex viscosity, nanofluid density, and nanofluid dynamic viscosity, respectively. Furthermore, $\check{n}$ stands for the micro gyration parameter; j is used for the micro inertia density, $\check{\alpha}_{nf}$ shows the thermal diffusivity, $\check{\gamma}_{nf}$ presents the spin gradient viscosity, $\check{T}$ displays the temperature; and $\check{N}$ is the micro rotation vector. Thus, by the well-known interpretation that the $\check{n}$ parameter varies in the closed interval $\check{n} \in [0, 1]$, whereas by special imposed condition $\check{n} = 0$ signifies the strong concentration, $\check{n} = 0.5$ suggests as weak concentration, and the turbulent flow is found for the value $\check{n} = 1$.

Using the Rosseland approximation, the radiative heat flux can be calculated as follows:

$$\check{q}_r + \frac{4\check{\sigma}^*}{3\check{k}^*}\frac{\partial \check{T}^4}{\partial \check{y}} = 0 \tag{6}$$

where $\check{\sigma}^*$ and $\check{k}^*$ denotes the constant of Stefan–Boltzmann and the coefficient of mean absorption. It is acknowledged that the flow is tiny in comprising the temperature differences, in showing that the mathematical formulation of $\left(\check{T}^2\right)^2$ may be articulated as a degree one function of temperature. Thus, by exercising the Taylors series for $\check{T}^4$ about a point $\check{T}_\infty$ and vanished the higher order term, we get Equation (7):

$$\left(\check{T}^2\right)^2 \approx -3T_\infty^4 + 2^2 T_\infty^3 T. \tag{7}$$

The standard of nanoparticles equations for $\check{\rho}_{nf}$, $\check{\alpha}_{nf}$, $(\rho c_p)_{nf}$, $\check{\mu}_{nf}$, k_{nf}/k_f,$\check{\gamma}_{nf}$, and $(\check{\rho}\check{\beta})_{nf}$ are as follows:

$$\begin{gathered}
\check{\rho}_{nf} + (\phi-1)\check{\rho}_f = \phi\check{\rho}_s,\ \check{\alpha}_{nf}\left(\check{\rho}\check{c}_p\right)_{nf} = \check{k}_{nf},\ \left(\check{\rho}\check{c}_p\right)_{nf} + (\phi-1)\left(\check{\rho}\check{c}_p\right)_f = \phi\left(\check{\rho}\check{c}_p\right)_s, \\
\check{\mu}_{nf} = \frac{\check{\mu}_f}{(1-\phi)^{2.5}},\ \frac{\check{k}_{nf}}{\check{k}_f} = \frac{\left(\check{k}_s+2\check{k}_f\right)-2\phi\left(\check{k}_f-\check{k}_s\right)}{\left(\check{k}_s+2\check{k}_f\right)+\phi\left(\check{k}_f-\check{k}_s\right)},\ \check{\gamma}_{nf} = \left(\check{\mu}_{nf} + \check{\kappa}/2\right)j, \\
\left(\check{\rho}\check{\beta}\right)_{nf} = (1-\phi)\left(\check{\rho}\check{\beta}\right)_f + \phi\left(\check{\rho}\check{\beta}\right)_s.
\end{gathered} \tag{8}$$

where ϕ stands for the nanoliquid volume fraction; $\check{k}_f$ and $\check{k}_s$ portray the thermal conductivity of regular liquid and nanoliquid; $\check{\rho}_s$ and $\check{\rho}_f$ show the density of nanoliquid and the base fluid; and $(\check{\rho}\check{\beta})_s$ and $(\check{\rho}\check{\beta})_f$ represent the thermal expansion of nanoliquid and base fluid coefficients, respectively.

We utilize the transformation called the similarity, as mentioned below, in Equation (9):

$$\begin{gathered}
u = c\check{x}F'(\eta),\ \eta = \check{y}\sqrt{\frac{c}{\nu_f}},\ v = -\sqrt{c\nu_f}\check{F}(\eta), \\
\check{N}(\eta) = c\check{x}\sqrt{\frac{c}{\nu_f}}G,\ \theta(\eta) = \frac{\check{T}-\check{T}_\infty}{\check{T}_w-\check{T}_\infty}.
\end{gathered} \tag{9}$$

By applying Equation (9), Equations (2) to (5), by utilizing Equations (6) to (8) are transmuted to the following equations:

$$\begin{gathered}
\left(\frac{1+(1-\phi)^{2.5}K}{(1-\phi)^{2.5}}\right)F''' + \left[(1-\phi)\left(FF'' - F'^2 + 1\right) + \phi\frac{\check{\rho}_s}{\check{\rho}_f}\left(FF'' - F'^2 + 1\right)\right] \\
+KG' + Qe^{-\Lambda\eta} + \lambda\left[(1-\phi) + \phi\frac{(\check{\rho}\check{\beta})_s}{(\check{\rho}\check{\beta})_f}\right]\theta = 0,
\end{gathered} \tag{10}$$

$$\left(\frac{2+(1-\phi)^{2.5}K}{2(1-\phi)^{2.5}}\right)G'' - K(2G+F'') + (FG'-F'G)\left[(1-\phi) + \phi\frac{\check{\rho}_s}{\check{\rho}_f}\right] = 0, \tag{11}$$

$$\frac{\check{k}_{nf}}{\check{k}_f}(1+R_d)\theta'' + \Pr\left[(1-\phi) + \phi\frac{\left(\check{\rho}\check{c}_p\right)_s}{\left(\check{\rho}\check{c}_p\right)_f}\right](F\theta' - F'\theta) = 0 \tag{12}$$

Along the renewed boundary conditions, we get the following calculations:

$$\begin{gathered}
F(0) = 0,\ G(0) = -\check{n}F''(0),\ F'(0) = 0,\ \theta(0) = 1 \text{ at } \eta = 0, \\
F'(\infty) \to 1,\ G(\infty) \to 0, \theta(\infty) \to 0 \text{ as } \eta \to \infty.
\end{gathered} \tag{13}$$

In overhead equations, dimensionless constant parameters and numbers are as follows: micropolar is K, buoyancy is λ, Grashof is Gr_x, Reynolds is Re_x radiation is R_d, modified Hartmann is Q, dimensionless is Λ, and Prandtl is $(\Pr)$.

$$K\check{\mu}_f = \check{\kappa},\ \lambda = gb\check{\beta}_f/c^2 = Gr_x/\mathrm{Re}_x^2,\ Gr_x\nu_f^2 - g\check{\beta}_f\left(\check{T}_w - \check{T}_\infty\right)\check{x}^3 = 0,\mathrm{Re}_x = \check{x}\check{u}_\infty(\check{x})/\nu_f,$$

$$R_d = 16\breve{\sigma}^*\breve{T}_\infty^3/3\breve{k}^*\breve{k}_{nf},\ Q = \pi J_0 M_0/8c^{3/2}\mathrm{Re}_x^{1/2}\breve{\rho}_f\sqrt{v_f},\Lambda = \pi\sqrt{v_f}/d\sqrt{c},\mathrm{Pr}\alpha_f = \nu_f,\nu_f = jc$$

The skin friction coefficient and the Nusselt number are calculated as follows:

$$C_{fx}\breve{\rho}_{nf}\breve{u}_\infty^2 = \left[\breve{\mu}_{nf}\frac{\partial\breve{u}}{\partial\breve{y}} + \breve{\kappa}\frac{\partial\breve{u}}{\partial\breve{y}} + \breve{\kappa}\breve{N}\right]_{\breve{y}=0}, -Nu_x\frac{\breve{k}_f\left(\breve{T}_w - \breve{T}_\infty\right)}{\breve{k}_{nf}} = \breve{x}\frac{\partial\breve{T}}{\partial\breve{y}}\bigg|_{\breve{y}=0} \tag{14}$$

Using Equations (8) and (9), we attain the following:

$$C_{fx}\mathrm{Re}_x^{1/2} = \frac{F''(0)}{\left[(1-\phi) + \phi\frac{\breve{\rho}_s}{\breve{\rho}_f}\right]}\left(\frac{1-(1-\phi)^{2.5}(\breve{n}-1)K}{(1-\phi)^{2.5}}\right), Nu_x\mathrm{Re}_x^{-1/2} = -\frac{\breve{k}_{nf}}{\breve{k}_f}\theta'(0) \tag{15}$$

3. Entropy Analysis

Analysis of entropy generation with micropolar fluid holding titanium alloy nanomaterial with thermal radiation is engraved as follows:

$$S_{gen}''' = \frac{1}{\breve{T}_\infty^2}\left(k_{nf} + \frac{16\breve{\sigma}^*\breve{T}_\infty^3}{3\breve{k}^*}\right)\left(\frac{\partial\breve{T}}{\partial\breve{y}}\right)^2 + \frac{1}{\breve{T}_\infty}\left(\breve{\mu}_{nf} + \breve{\kappa}\right)\left(\frac{\partial\breve{u}}{\partial\breve{y}}\right)^2 \tag{16}$$

Volumetric entropy number is characterized as follows:

$$S_0''' = \frac{k_f\left(\Delta\breve{T}\right)^2}{L^2\breve{T}_\infty^2} \tag{17}$$

In dimensionless form, we get Equation (8):

$$N_G = \frac{S_{gen}'''}{S_0'''} = \frac{\mathrm{Re}_L Br}{\Omega}\left(\frac{1+(1-\phi)^{2.5}K}{(1-\phi)^{2.5}}\right)F''^2 + \frac{\breve{k}_{nf}}{\breve{k}_f}\mathrm{Re}_L(1+R_d)\theta\theta'^2 \tag{18}$$

where $\Omega = \Delta\breve{T}/\breve{T}_\infty$ is the dimensionless difference of temperature, $Br = \breve{\mu}_f\breve{u}_c^2/k_f\Delta\breve{T}$ is the Brinkman number, and $\mathrm{Re}_L = cL^2/\nu_f$ is the characteristic length based Reynolds number.

4. Results and Discussions

The transmuted mixed convective problem described in Equations (10) to (12) through boundary condition in Equation (13) has been computed numerically via the formula of three-stage Lobatto IIIA. The influences of physical parameters on velocity and micro-rotation profiles, temperature distribution, along with the corresponding $Nu_x\mathrm{Re}_x^{-1/2}$ and $C_{fx}\mathrm{Re}_x^{1/2}$, is established and portrayed graphically via Figures 2–22. Now, at this point, we can take the value of the micro gyration parameter is equal to 0.5. The feature properties of the regular and particle fluids are exemplified in Table 1. The authenticity of our computational results were invoked in Tables 2 and 3 for $F''(0)$ and $-\theta'(0)$, and we found a tremendous agreement as compared to old one.

Table 1. Thermophysical properties of base fluid and Ti_6Al_4V.

Material	Water	Ti_6Al_4V
$C_p(J/kgK)$	4179	0.56
$\rho\left(kg/m^3\right)$	997.1	4420
$k(W/mK)$	0.613	7.2
$\beta\times10^{-5}(1/K)$	21	5.8
Pr	6.2	-

Table 2. Comparison of $F''(0)$ when $\lambda = 1, \phi = 0, K = 0, Q = 0$.

Pr	Lok et al. [3]	Aman et al. [4]	Present
0.7	1.7064	1.7063	1.7063
1	-	1.6754	1.6754
7	1.5180	1.5179	1.5179
10	-	1.4928	1.4928
20	1.4486	1.4485	1.4485
40	1.4102	1.4101	1.4101
50	-	1.3989	1.3989
60	1.3903	1.3903	1.3903
80	1.3773	1.3773	1.3776
100	1.3677	1.3680	1.3683

Table 3. Comparison of $-\theta'(0)$ when $\lambda = 1, \phi = 0, K = 0, Q = 0$.

Pr	Lok et al. [3]	Aman et al. [4]	Present
0.7	0.7641	0.7641	0.7641
1	-	0.8708	0.8708
7	1.7226	1.7224	1.7224
10	-	1.9446	1.9446
20	2.4577	2.4476	2.4576
40	3.1023	3.1011	3.1011
50	-	3.3415	3.3415
60	3.5560	3.5514	3.5515
80	3.9195	3.9095	3.9097
100	4.2289	4.2116	4.2120

Figures 2–4 observe the impression of micropolar parameter K on micro rotation, velocity profiles, and temperature distribution. The larger values of K decline $F'(\eta)$ and micro-rotation fields in the upper-branch solution, as well as in the second-branch solution, while the temperature distribution augments for K in both solutions. Physically, due to escalating viscosity, microelements therefore continuously encourage and slowdown in the flow nearby the plate. From these plots, the significant growth in the behavior of thermal and momentum boundary layer thicknesses is noticed as K grows in first and second solutions. It is also perceived that the plots are larger in non-viscous liquid $(K \neq 0)$ compared to viscous liquid $(K = 0)$.

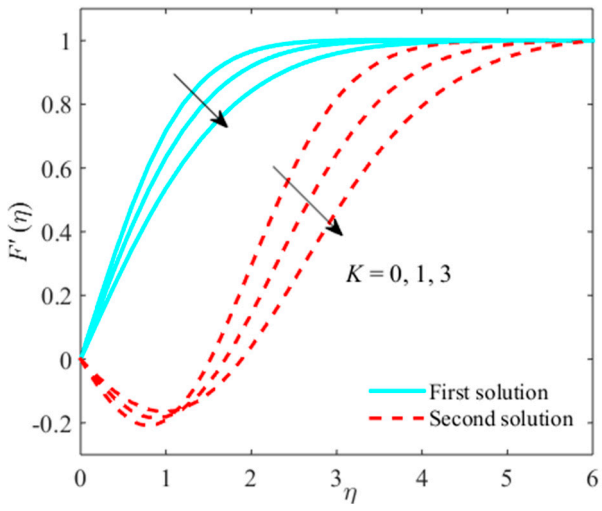

Figure 2. Impact of K on $F'(\eta)$ when $\phi = 0.01, Q = 0.01, \gamma = 0.1, \lambda = -0.2, R_d = 0.2$.

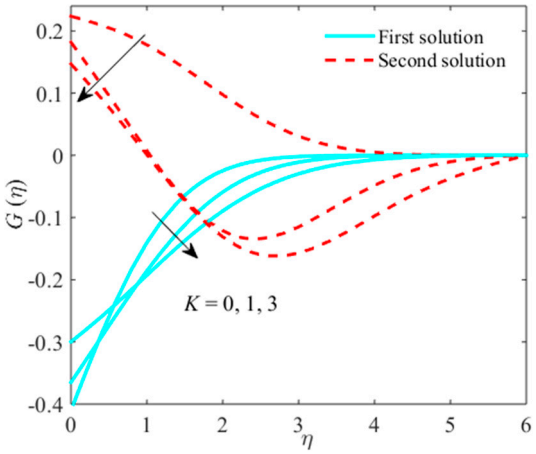

Figure 3. Impact of K on $G(\eta)$ when $\phi = 0.01, Q = 0.01, \gamma = 0.1, \lambda = -0.2, R_d = 0.2$.

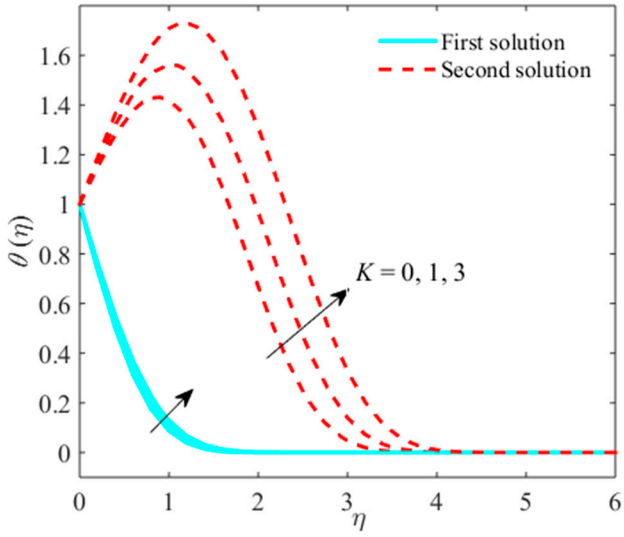

Figure 4. Impact of K on $\theta(\eta)$ when $\phi = 0.01, Q = 0.01, \gamma = 0.1, \lambda = -0.2, R_d = 0.2$.

Figures 5–7 are enlisted in pursuit of the stimulation of ϕ on liquid $F'(\eta)$, micro rotation, and temperature fields. Figure 5 explains that the liquid velocity shrinks when ϕ rises in the first solution, while the graph shows escalating behavior in the second solution. Physically, it indicates that the ϕ raises the k, which consequently shrinks the momentum boundary layer. However, the graph of micro rotation (Figure 6) displays a decreasing trend with the enhancement of ϕ in both branches. In contrast, the temperature (Figure 7) and boost-up thermal boundary layer due to ϕ in upper solution while in lower solution reverse trend is examined. This means that ϕ improves the element-to-element distribution. Physically, as the ϕ of titanium alloy nanomaterial grows the thermal conductivity, it improves the thermal boundary layer by making it finer in the upper branch. The variations in the material, size, shape, and concentration nanoparticles, allow for alteration to boost up the energy of absorption, using via the volume of fluid, since the ϕ depends on the magnitude of the particle. Escalating the ϕ results in raising the coefficient of heat transfer.

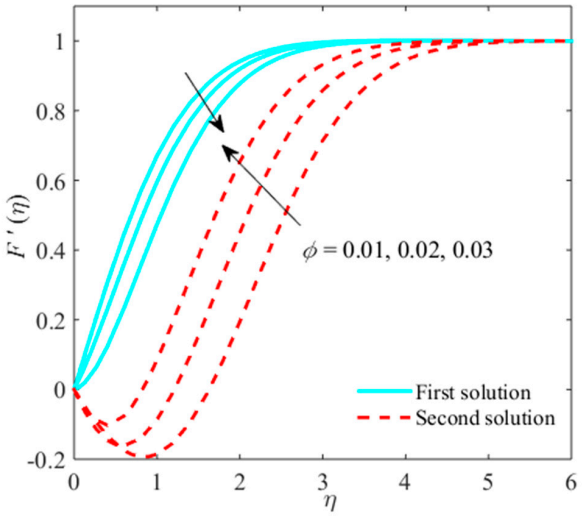

Figure 5. Impact of ϕ on $F'(\eta)$ when $K = 0.5, Q = 0.01, \gamma = 0.1, \lambda = -0.2, R_d = 0.2$.

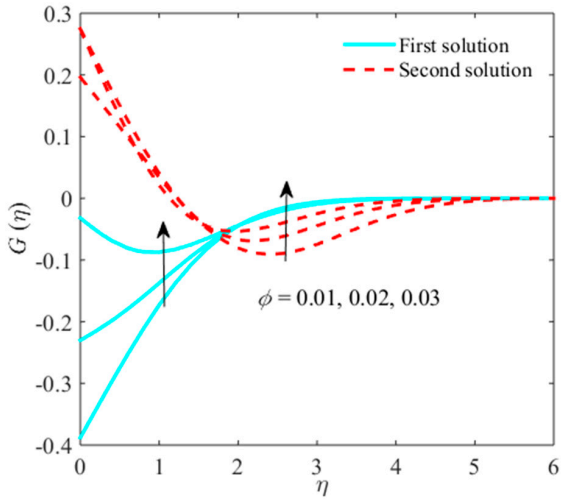

Figure 6. Impact of ϕ on $G(\eta)$ when $K = 0.5, Q = 0.01, \gamma = 0.1, \lambda = -0.2, R_d = 0.2$.

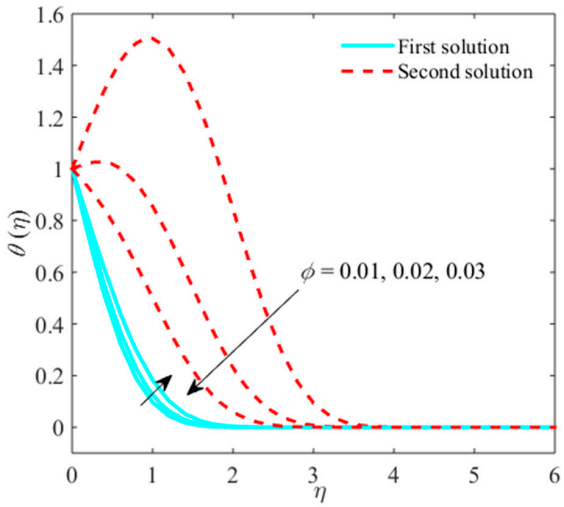

Figure 7. Impact of ϕ on $\theta(\eta)$ when $K = 0.5, Q = 0.01, \gamma = 0.1, \lambda = -0.2, R_d = 0.2$.

Another significant factor in our study is the modified Hartman number, Q, which is portrayed in Figures 8–10. Figure 8 captures that the liquid velocity enhances from mounting the values of Q in both branches. This means that various selected choices of Q outcomes which augment internal or external forces called adhesive and cohesive forces. Due to these forces, the momentum of the flow is increased, and thus, as a result, the velocity expands. On the other hand, the micro-rotation plot shows the opposite behavior when Q increases, as shown in Figure 9. Figure 10 elucidates that the liquid temperature moderates with higher choices of Q in upper solution and develops in lower branch. Physically, outer/inner forces present an additional resistance to stop the flow of fluid particles. Therefore, more heat is formed, which, in turn, enhances the second branch solution for the temperature distribution.

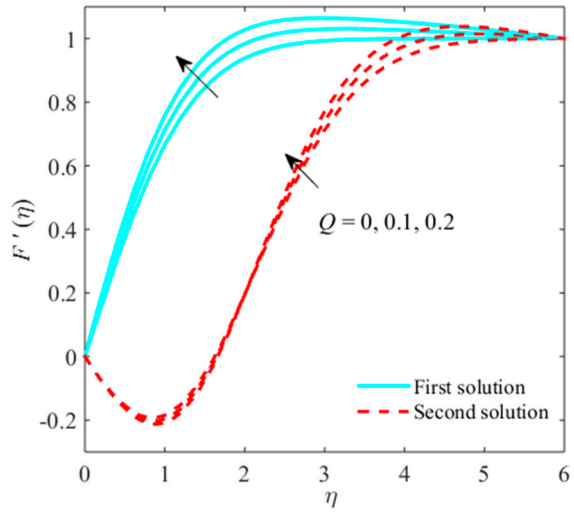

Figure 8. Impact of Q on $F'(\eta)$ when $K = 0.5, \phi = 0.01, \gamma = 0.01, \lambda = -0.2, R_d = 0.2$.

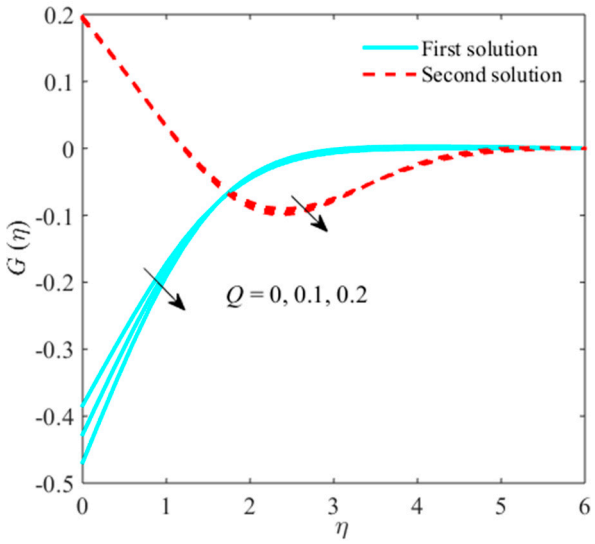

Figure 9. Impact of Q on $G(\eta)$ when $K = 0.5, \phi = 0.01, \gamma = 0.01, \lambda = -0.2, R_d = 0.2$.

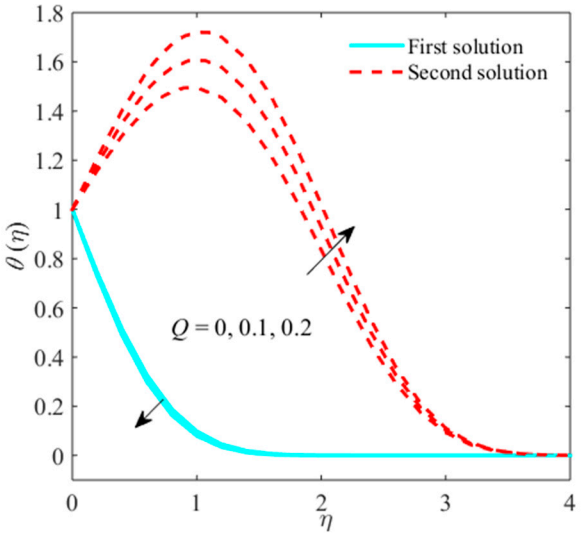

Figure 10. Impact of Q on $\theta(\eta)$ when $K = 0.5, \phi = 0.01, \gamma = 0.01, \lambda = -0.2, R_d = 0.2$.

Figures 11–13 are organized to examine the stimulus of R_d on $F'(\eta)$, micro rotation, and temperature fields. An anticipated result from these outcomes is that the momentum, thermal boundary layers, and micro rotation thicknesses increase as radiation parameter grows. Physically, it shows that the radiation impact is augmented due to more heat of flux as a result the higher temperature, which is observed within the boundary layer region. Moreover, at all times, it is susceptible to preserve the minimum thermal radiation to achieve a higher rate of heat transfer, which leads toward additional cooling.

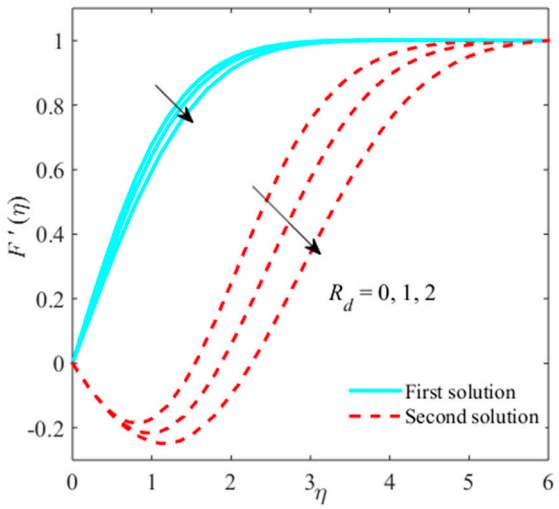

Figure 11. Impact of R_d on $F'(\eta)$ when $K = 0.5, \phi = 0.01, Q = 0.01, \gamma = 0.1, \lambda = -0.2$.

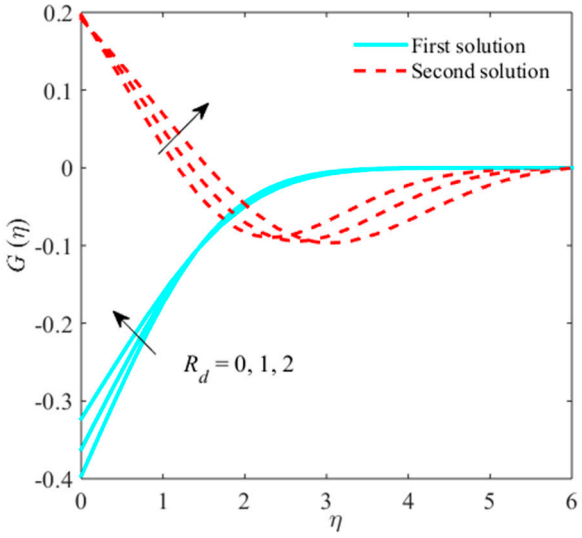

Figure 12. Impact of R_d on $G(\eta)$ when $K = 0.5, \phi = 0.01, Q = 0.01, \gamma = 0.1, \lambda = -0.2$.

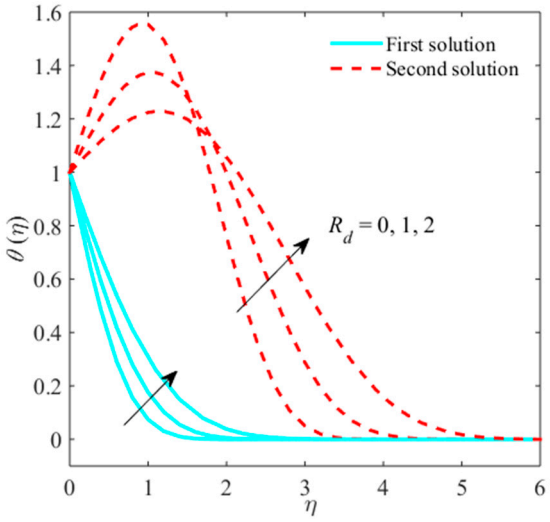

Figure 13. Impact of R_d on $\theta(\eta)$ when $K = 0.5, \phi = 0.01, Q = 0.01, \gamma = 0.1, \lambda = -0.2$.

The impacts of ϕ, micropolar parameter, Reynolds number, and radiation parameter on entropy generation are sketched in Figures 14–17. Figure 14 explains that the entropy generation confirms the growing behavior due to ϕ in first outcome, while, in second outcome, the generation of entropy shrinks. Figure 15 shows that the entropy generation improves with superior behavior in both branches of solution due to boost-up K. It is imperative to observe that plot of entropy generation is larger in K, not equal to zero compared to K equal to zero. Figure 16 reveals that the entropy generation is caused by enhancing the Reynolds number. Physically, the entropy formed from all irreversibility mechanisms, and thus entropy enhances due to the Reynolds number. Figure 17 depicts that, for a larger radiation parameter, the entropy generation is enhanced. For the superior belief of R_d systems, internal energy augments, making it accountable for rising the entropy generation. The intention of Brinkman number is to find the rate of heat releasing through molecular conduction to viscous heating. The greater amount of heat discharges involved liquid particle layers, which are accountable for enhancing the entropy generation, as shown in Figure 18.

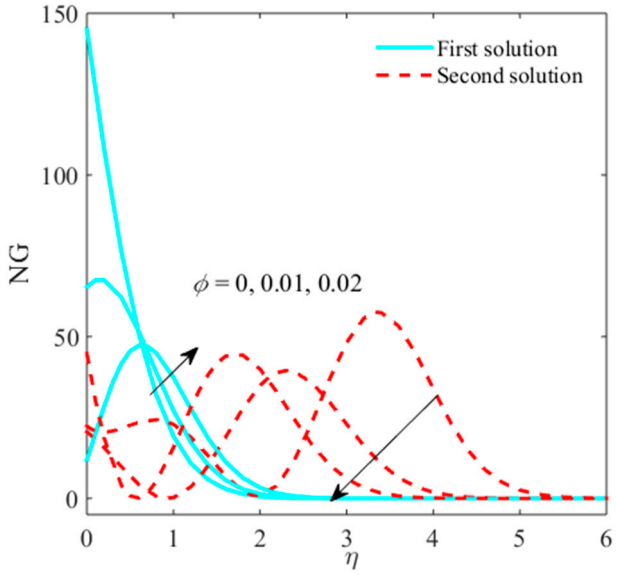

Figure 14. Impact of ϕ on NG when $K = 0.1, Q = 0.01, \gamma = 0.1, R_d = 1, \lambda = -0.2$, $\mathrm{Re}_L = Br = 1$, $\Omega = 0.01$.

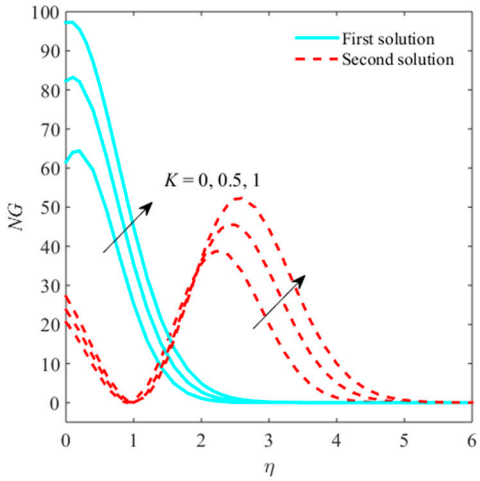

Figure 15. Impact of K on NG when $\phi = 0.01, Q = 0.01, \gamma = 0.1, R_d = 1, \lambda = -0.2$, $\mathrm{Re}_L = Br = 1$, $\Omega = 0.01$.

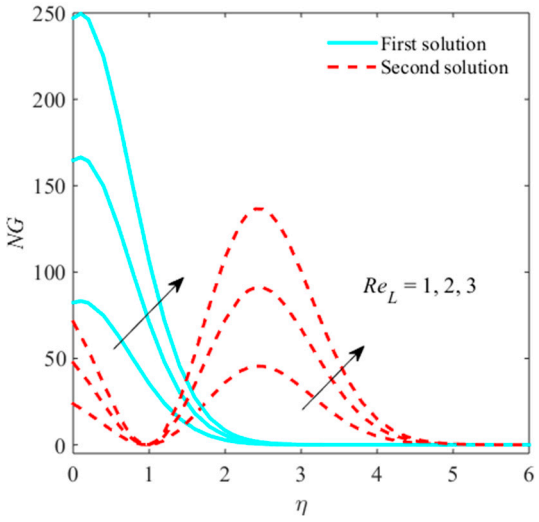

Figure 16. Impact of Re_L on NG when $K = 0.1, \phi = Q = 0.01, \gamma = 0.1, R_d = 1, \lambda = -0.2$, $Br = 1$, $\Omega = 0.01$.

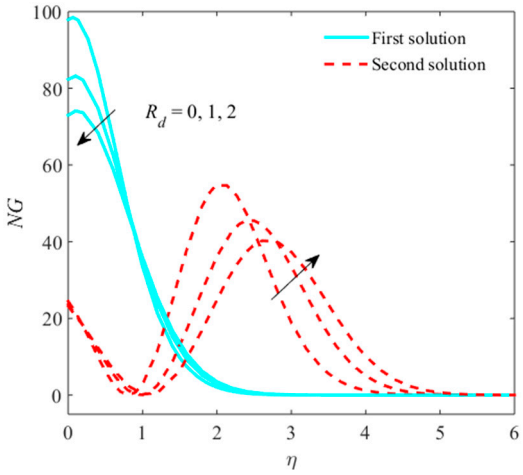

Figure 17. Impact of R_d on NG when $K = 0.5, \phi = Q = 0.01, \gamma = 0.1, \lambda = -0.2, \mathrm{Re}_L = Br = 1, \Omega = 0.01$.

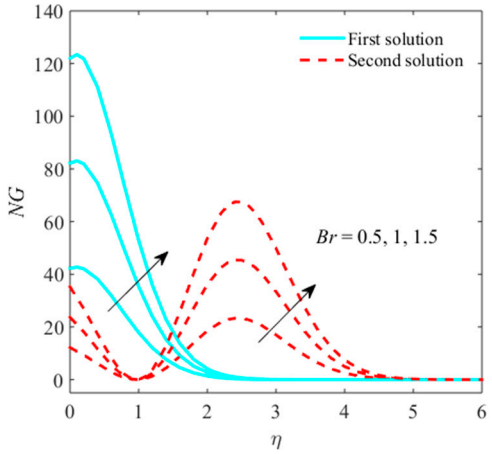

Figure 18. Impact of Br on NG when $K = 0.5, \phi = Q = 0.01, \gamma = 0.1, \lambda = -0.2, R_d = \mathrm{Re}_L = 1, \Omega = 0.01$.

Figures 19 and 20 are set to view the effect of micropolar K on the $C_{fx}\mathrm{Re}_x^{1/2}$ and the $Nu_x\mathrm{Re}_x^{-1/2}$ versus mixed convective parameter λ. The (dual) more than one solution is accomplished for the case

of opposing flow ($\lambda < 0$), while the solution is unique in the case of assisting flow ($\lambda > 0$). The multiple solutions exist in some range where the critical values are found, and their values are mentioned in the graphs for λ (say λ_c), and no solution exists in the range $\lambda > \lambda_c$. $\lambda = \lambda_c$ is the point where both solutions are combined or the same. Computationally, we tackled our problem and found the values of λ_c are -0.5219, -0.5520, and -0.5783 for the different values of K equal to 0, 0.5, 1, respectively. Therefore, the values of $|\lambda_c|$ grow with bigger values of K. The separation of the boundary layer is decaying due to micropolar parameters. In addition, the values of skin friction in the first branch enhance as K and λ rise, while the opposite trend is scrutinized in the second solution. Physically, assisting flow generated an auspicious pressure slope that augmented the movement of fluid, which successively boosted the shear stress at the surface of the plate. In spite of this, the values of the Nusselt number shows a declining behavior with mounting values of K in uphill and downhill solution, because an adverse velocity slope yields by opposing flow, which delays the run of fluid.

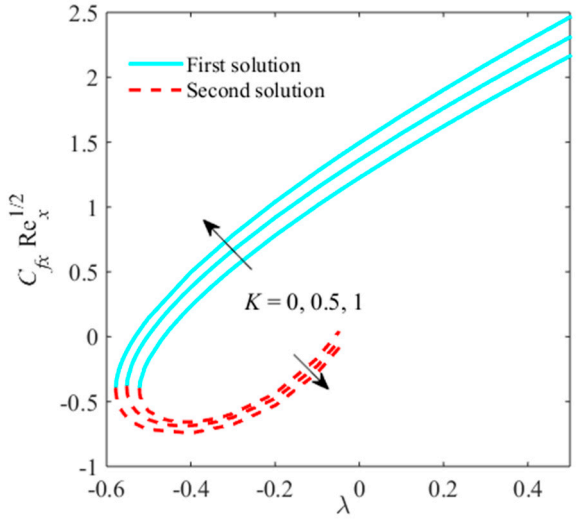

Figure 19. Impact of K on $C_{fx}\mathrm{Re}_x^{1/2}$ when $\phi = Q = 0.01, \gamma = 0.1, R_d = 0.5$.

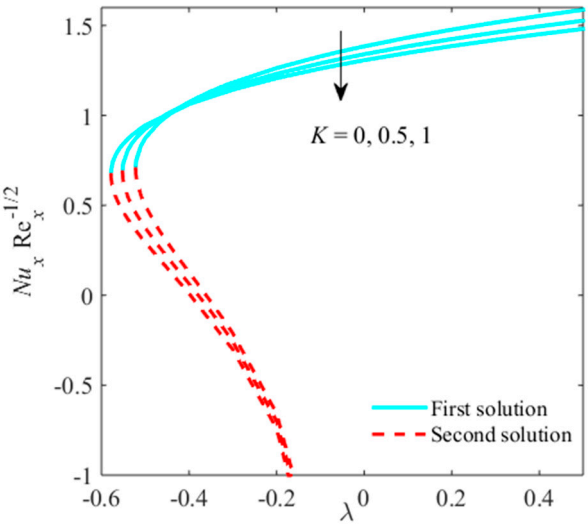

Figure 20. Impact of K on $Nu_x\mathrm{Re}_x^{-1/2}$ when $\phi = Q = 0.01, \gamma = 0.1, R_d = 0.5$.

Figures 21 and 22 explain the patterns of streamlines in first and second solutions. Figure 21 indicates that the flow pattern of lines is symmetric, fuller, and simple from an axis in uphill solution, due to equal forces of opposing and assisting flows. Alternatively, Figure 22 demonstrates that the streamlines are somewhat complex in upper solution and part the flows in the double region.

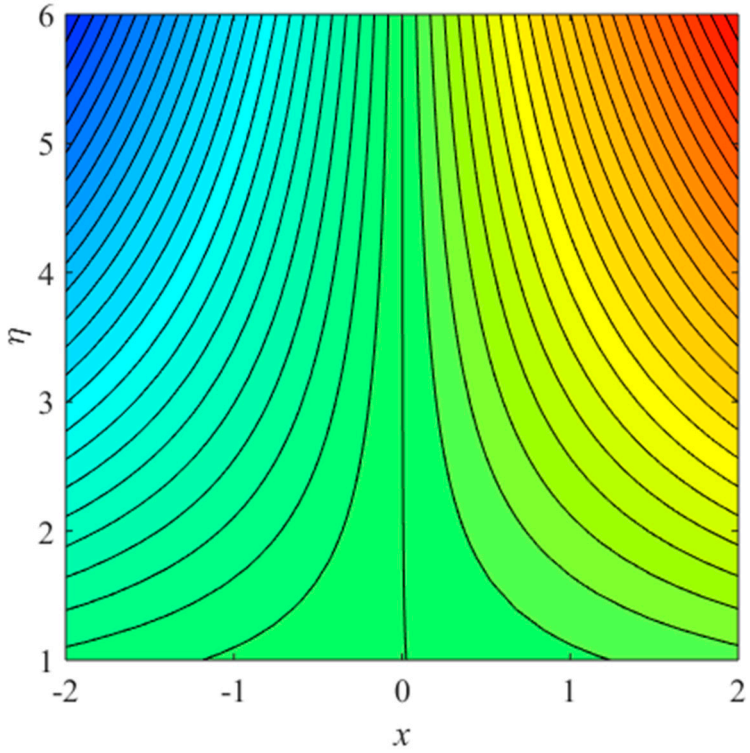

Figure 21. Streamline patterns for first solution when $K = 0.5, \phi = Q = 0.01, \gamma = 0.1, \lambda = -0.2$.

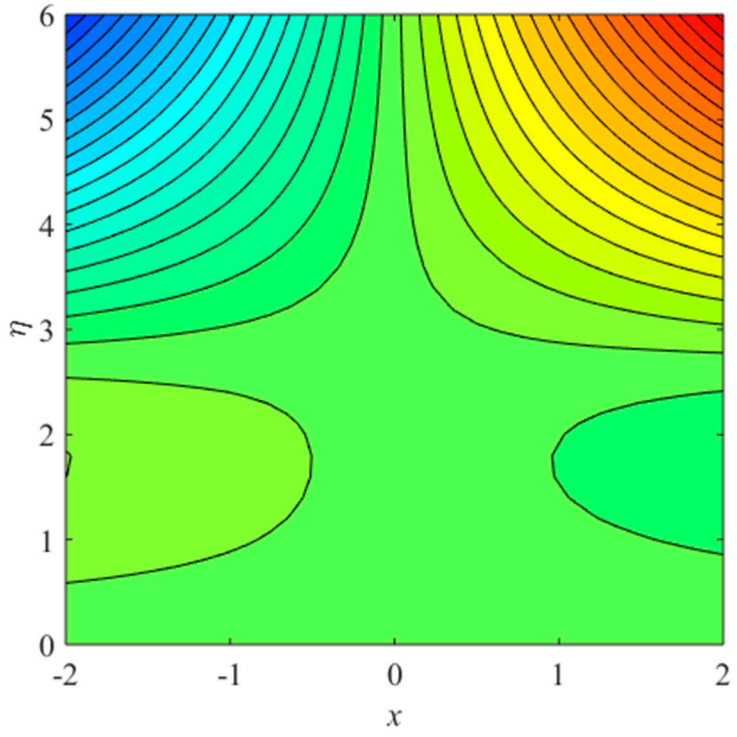

Figure 22. Streamline patterns for second solution when $K = 0.5, \phi = Q = 0.01, \gamma = 0.1, \lambda = -0.2$.

5. Concluding Remarks

Here, the impact of thermal radiation on mixed convection flow of micropolar liquid comprising titanium alloy nanomaterial over a Riga plate with entropy generation is discussed. More than one

solution is obtained in opposing flow by using the formula of three-stage Lobatto IIIA. The key points monitored from the current flow problem are enlisted below:

- ➢ The dual solutions are attained in opposing flow only.
- ➢ Increasing the micropolar parameter decreases the liquid velocity and micro rotation and raises the temperature distribution within the region of boundary layer in both branches.
- ➢ Micropolar parameter impedes the boundary layer separation.
- ➢ Velocity and micro rotation fields augment for escalating values of ϕ in the second solution, while in the first solution, the reverse behavior is seen. Temperature field rises in the upper solution and falloffs in the lower solution due to ϕ
- ➢ The results exposed that liquid velocity is accelerated and micro rotation is decelerated by modified Hartmann number in both solutions, whereas temperature field is decelerated in the uphill solution and accelerated in the downhill solution.
- ➢ Radiation parameter enhances the temperature and micro rotation fields and reduces the liquid velocity in both solutions.
- ➢ Increasing behavior is observed for an entropy generation in both solutions via K, Re_L, and Br. In contrast, an entropy generation augments due to ϕ and declines due to R_d in the first solution.

Author Contributions: A.Z. and U.K. conceived and designed the model; I.K. performed the formulation; A.H.S. and E.-S.M.S. analyzed the data; A.Z. contributed reagents/materials/analysis tools; U.K. wrote the paper. All authors have read and agreed to the published version of the manuscript.

Funding: This research is funded from the Project number (RSP-2019/33), King Saud University, Riyadh, Saudi Arabia.

Acknowledgments: Researchers Supporting Project number (RSP-2019/33), King Saud University, Riyadh, Saudi Arabia.

Conflicts of Interest: Authors do not have any conflict of interest.

Nomenclature

b, c	positive constants
C_{fx}	skin friction coefficient
c_p	specific heat of fluid [J kg^{-1} K^{-1}]
d	electrodes and magnets width
g	acceleration caused by gravity [ms^{-2}]
Gr_x	Grashof number
J_0	applied current density in the electrodes
j	micro inertia per unit mass [m^2]
K	micropolar parameter
$\breve{k}^*$	absorption coefficient
$\breve{k}_f$	thermal conductivity of regular liquid [W m^{-1} K^{-1}]
$\breve{k}_s$	thermal conductivity of nanoliquid [W m^{-1} K^{-1}]
$\breve{M}_0$	magnetization of thepermanents magnets
$\breve{N}$	micro rotation vector [ms^{-1}]
$\breve{n}$	micro gyration parameter
Nu_x	Nusselt number
Pr	Prandtl number
$\breve{q}_r$	radiative heat flux [W m^{-2}]
R_d	radiation parameter
Re_x	local Reynolds number
$\breve{T}$	temperature [T]
$\breve{T}_\infty$	free stream temperature [T]
$\breve{T}_w$	fluid temperature at wall [T]

$\breve{u}_\infty$	free stream velocity [ms^{-1}]
$\breve{u}, \breve{v}$	velocity components [ms^{-1}]
$\breve{x}, \breve{y}$	Cartesian coordinates [m]
Greek symbols	
Q	modified Hartmann number
$\breve{\alpha}_{nf}$	thermal diffusivity [m^2 s^{-1}]
β_{nf}	nanofluid thermal expansion [K^{-1}]
$\breve{\gamma}_{nf}$	spin−gradient viscosity [kg m s^{-1}]
$\breve{\kappa}$	vortex viscosity [kg m^{-1} s^{-1}]
λ	mixed convective parameter
$\breve{\mu}_{nf}$	nanofluid dynamic viscosity [kg m^{-1} s^{-1}]
ϕ	volume fraction of nanoliquid
θ	dimensionless temperature
ν_f	kinematic viscosity [m^2 s^{-1}]
$\breve{\rho}_{nf}$	density [kg m^{-3}]
$\breve{\rho}_s$	density of nanoliquid [kg m^{-3}]
$\breve{\rho}_f$	density of base fluid [kg m^{-3}]
ψ	stream function [m^2 s^{-1}]
Λ	dimensionless parameter
$\breve{\sigma}^*$	Stefan–Boltzmann constant [Wm^{-2}K^{-4}]
η	similarity variable
Subscripts	
w	condition at wall
∞	condition at free stream
Superscripts	
$'$	derivative w.r.t. η

References

1. Eringen, A.C. Theory of micropolar fluids. *J. Appl. Math. Mech.* **1966**, *16*, 1–18. [CrossRef]
2. Mohammadein, A.A.; Gorla, R.S.R. Heat transfer in a micropolar fluid over a stretching sheet with viscous dissipation and internal heat generation. *Int. J. Numer. Methods Heat Fluid Flow* **2001**, *11*, 50–58. [CrossRef]
3. Lok, Y.Y.; Amin, N.; Pop, I. Unsteady mixed convection flow of a micropolar fluid near the stagnation point on a vertical surface. *Int. J. Thermal Sci.* **2006**, *45*, 1149–1157. [CrossRef]
4. Aman, F.; Ishak, A.; Pop, I. Mixed convection boundary layer flow near stagnation-point on vertical surface with slip. *Appl. Math. Mech. Engl. Ed.* **2011**, *32*, 1599–1606. [CrossRef]
5. Turkyilmazoglu, M. Flow of a micropolar fluid due to a porous stretching sheet and heat transfer. *Int. J. Non-Linear Mech.* **2016**, *83*, 59–64. [CrossRef]
6. Hussanan, A.; Salleh, M.Z.; Khan, I.; Tahar, R.M. Unsteady free convection flow of a micropolar fluid with Newtonian heating: Closed form solution. *Therm. Sci.* **2017**, *21*, 2313–2326. [CrossRef]
7. Waqas, H.; Hussain, S.; Sharif, H.; Khalid, S. MHD forced convective flow of micropolar fluids past a moving boundary surface with prescribed heat flux and radiation. *Br. J. Math. Comput. Sci.* **2017**, *21*, 1–14. [CrossRef]
8. Das, K.; Duari, P.R. Micropolar nanofluid flow over a stretching sheet with chemical reaction. *Int. J. Appl. Comput. Math.* **2017**, *3*, 3229–3239. [CrossRef]
9. Hsiao, K.L. Micropolar nanofluid flow with MHD and viscous dissipation effects towards a stretching sheet with multimedia feature. *Int. J. Heat Mass Transf.* **2017**, *112*, 983–990. [CrossRef]
10. Hussanan, A.; Salleh, M.Z.; Khan, I.; Tahar, R.M. Heat and mass transfer in a micropolar fluid with Newtonian heating: An exact analysis. *Neural Comput. Appl.* **2018**, *29*, 59–67. [CrossRef]
11. Makinde, O.D.; Aziz, A. Boundary layer flow of a nanofluid past a stretching sheet with a convective boundary condition. *Int. J. Therm. Sci.* **2011**, *50*, 1326–1332. [CrossRef]
12. Hogan, C. Density of states of an insulating ferromagnetic alloy. *Phys. Rev.* **1969**, *188*, 870. [CrossRef]
13. Parayanthal, P.; Pollak, F.H. Raman scattering in alloy semiconductors: Spatial correlation model. *Phys. Rev. Lett.* **1984**, *52*, 1822–1825. [CrossRef]

14. Žitňanský, M.; Čaplovič, L. Effect of the thermomechanical treatment on the structure of titanium alloy Ti_6Al_4V. *J. Mater. Process. Technol.* **2004**, *157*, 643–649. [CrossRef]
15. Zhu, X.J.; Tan, M.J.; Zhou, W. Enhanced super plasticity in commercially pure titanium alloy. *Scr. Mater.* **2005**, *52*, 651–655. [CrossRef]
16. Hao, Y.L.; Li, S.J.; Sun, B.B.; Sui, M.L.; Yang, R. Ductile titanium alloy with low Poisson's ratio. *Phys. Rev. Lett.* **2007**, *98*, 216405. [CrossRef]
17. Balazic, M.; Kopac, J.; Jackson, M.J.; Ahmed, W. Review: Titanium and titanium alloy applications in medicine. *Int. J. Nano Biomater.* **2007**, *1*, 3–34. [CrossRef]
18. Raju, C.S.K.; Sekhar, K.R.; Ibrahim, S.M.; Lorenzini, G.; Reddy, G.V.; Lorenzini, E. Variable viscosity on unsteady dissipative Carreau fluid over a truncated cone filled with titanium alloy nanoparticles. *Contin. Mech. Thermodyn.* **2017**, *29*, 699–713. [CrossRef]
19. Kassai, M.; Poleczky, L.; Al-Hyari, L.; Kajtar, L.; Nyers, J. Investigation of the Energy Recovery Potentials in Ventilation Systems in Different Climates. *Facta Univ. Ser. Mech. Eng.* **2018**, *16*, 203–217. [CrossRef]
20. Gao, H.; Guo, L.J.; Zhang, X.M. Liquid-solid separation phenomena of two-phase turbulent flow in curved pipes. *Int. J. Heat Mass Transf.* **2002**, *45*, 4995–5005. [CrossRef]
21. Kassai, M.; Ge, G.; Simonson, C.J. Dehumidification performance investigation of run-around membrane energy exchanger system. *Therm. Sci.* **2016**, *20*, 1927–1938. [CrossRef]
22. Shi, D.P.; Luo, Z.H.; Zheng, Z.W. Numerical simulation of liquid-solid two-phase flow in a tubular loop polymerization reactor. *Powder Technol.* **2010**, *198*, 135–143. [CrossRef]
23. Maxwell, J.C. *A Treatise on Electricity and Magnetism*, 2nd ed.; Clarendon Press: Oxford, UK, 1873; Volume 1.
24. Choi, S.U.S.; Eastman, J.A. Enhancing thermal conductivity of fluids with nanoparticles, developments and applications of non-Newtonian flows. In Proceedings of the 1995 International Mechanical Engineering Congress and Exhibition, San Francisco, CA, USA, 12–17 November 1995; Volume 66, pp. 99–105.
25. Khan, W.; Pop, I. Boundary-layer flow of a nanofluid past a stretching sheet. *Int. J. Heat Mass Transf.* **2010**, *53*, 2477–2483. [CrossRef]
26. Mabood, F.; Shateye, S.; Rashidi, M.M.; Momoniat, E.; Freidoonimehr, N. MHD stagnation point flow heat and mass transfer of nanofluids in porous medium with radiation, viscous dissipation and chemical reaction. *Adv. Powder Technol.* **2016**, *27*, 742–749. [CrossRef]
27. Hayat, T.; Qayyum, S.; Imtiaz, M.; Alsaedi, A. Comparative study of silver and copper water nanofluids with mixed convection and non-linear thermal radiation. *Int. J. Heat Mass Transf.* **2016**, *102*, 723–732. [CrossRef]
28. Du, M.; Tang, G.H. Plasmonic nanofluids based on gold nanorods/nanoellipsoids/nanosheets for solar energy harvesting. *Sol. Energy* **2016**, *137*, 393–400. [CrossRef]
29. Zaib, A.; Abelman, S.; Chamkha, A.J.; Rashidi, M.M. Entropy generation in a Williamson nanofluid near a stagnation point over a moving plate with binary chemical reaction and activation energy. *Heat Transf. Res.* **2018**, *49*, 1131–1149. [CrossRef]
30. Gailitis, A.; Lielausis, O. On a possibility to reduce the hydrodynamic resistance of a plate in an electrolyte. *Appl. Magnetohydrodyn. Rep. Phys. Inst. Riga* **1961**, *12*, 143–146.
31. Pantokratoras, A.; Magyari, E. EMHD free-convection boundary-layer flow from a Riga-plate. *J. Eng. Math.* **2009**, *64*, 303–315. [CrossRef]
32. Abbas, T.; Ayub, M.; Bhatti, M.M.; Rashidi, M.M.; Ali, M.E.l. Entropy generation on nanofluid flow through a horizontal Riga plate. *Entropy* **2016**, *18*, 223. [CrossRef]
33. Hayat, T.; Khan, M.; Imtiaz, M.; Alsaedi, A. Squeezing flow past a Riga plate with chemical reaction and convective conditions. *J. Mol. Liq.* **2017**, *225*, 569–576. [CrossRef]
34. Iqbal, Z.; Azhar, E.; Mehmood, Z.; Maraj, E.N. Melting heat transport of nanofluidic problem over a Riga plate with erratic thickness: Use of Keller Box scheme. *Res. Phys.* **2017**, *7*, 3648–3658. [CrossRef]
35. Bejan, A. A study of entropy generation in fundamental convective heat transfer. *J. Heat Transf.* **1979**, *101*, 718–725. [CrossRef]
36. Aiboud, S.; Saouli, S. Entropy analysis for viscoelastic magneto-hydrodynamic flow over a stretching surface. *Int. J. Non-linear Mech.* **2010**, *45*, 482–489. [CrossRef]
37. Butt, A.S.; Munawar, S.; Ali, A.; Mehmood, A. Entropy generation in hydrodynamic slip flow over a vertical plate with convective boundary. *J. Mech. Sci. Technol.* **2012**, *26*, 2977–2984. [CrossRef]

38. Noghrehabadi, A.; Saffarian, M.R.; Pourrajab, R.; Ghalambaz, M. Entropy analysis for nanofluid flow over a stretching sheet in the presence of heat generation/absorption and partial slip. *J. Mech. Sci. Technol.* **2013**, *27*, 927–937. [CrossRef]
39. Abolbashari, M.H.; Freidoonimehr, N.; Nazari, F.; Rashidi, M.M. Analytical modeling of entropy generation for Casson nano-fluid flow induced by a stretching surface. *Adv. Powder Technol.* **2015**, *26*, 542–552. [CrossRef]
40. Rehman, S.U.; Haq, R.U.; Khan, Z.H.; Lee, C. Entropy generation analysis for non-Newtonian nanofluid with zero normal flux of nanoparticles at the stretching surface. *J. Taiwan Inst. Chem. Eng.* **2016**, *63*, 226–235. [CrossRef]
41. Azhar, W.A.; Vieru, D.; Fetecau, C. Entropy generation due to fractional Couette flow in a rotating channel with exponential heating of walls. *Heat Transf. Res.* **2018**, *49*, 1507–1526. [CrossRef]
42. Hayat, T.; Khan, M.; Khan, M.I.; Alsaedi, A.; Ayub, M. Electromagneto squeezing rotational flow of carbon (C)-water (H_2O) kerosene oil nanofluid past a Riga plate: A numerical study. *PLoS ONE* **2017**, *12*, e0180976. [CrossRef]
43. Zaib, A.; Haq, R.U.; Chamkha, A.J.; Rashidi, M.M. Impact of partial slip on mixed convective flow towards a Riga plate comprising micropolar TiO_2-kerosene/water nanoparticles. *Int. J. Numer. Meth. Heat Fluid Flow* **2019**, *29*, 1647–1662. [CrossRef]